

## VI. Magnetic Materials

Magnetic fields are generated by moving electric charge. A current  $I$  flowing in a coil of  $n$  turns per meter produces a magnetic field  $H = nI$  amperes/meter.

All materials respond to a magnetic field, producing a magnetization  $M = \chi H$ , expressed in weber/m<sup>2</sup>. A weber is the unit of magnetic charge, weber-m of magnetic dipole moment, and weber/m<sup>2</sup> of magnetic dipole moment per unit volume (magnetization). Every dipole has its moment, just as every dog has his day. The magnetic susceptibility  $\chi$  is in henry/m but is usually presented as a dimensionless quantity  $\bar{\chi} = \chi/\mu_0$ , where  $\mu_0 = 4\pi \times 10^{-7}$  henry/m is the permeability of vacuum. Observed values of the relative susceptibility  $\bar{\chi}$  range from  $10^{-5}$  in weakly magnetic materials to  $10^6$  in strong magnets [1].  $\bar{\chi}$  may be linear or non-linear, and positive or negative and is often temperature-sensitive. It provides a convenient measure of the response of a material to an applied field, a response which is interpreted in terms of magnetic structure and electronic configurations.

Most materials are *diamagnetic*, a weak magnetic response induced by an applied magnetic field. In most compounds the electrons are paired in bonding, but magnetic fields cause small changes in orbital motion which result in a small negative susceptibility ( $\bar{\chi} \sim 10^{-5}$ ). Induced currents enclose larger areas in organic molecules giving larger effects. In a field gradient diamagnetic materials experience a force driving them out of the field.

Magnetization is also linearly proportional to field in *paramagnetic* materials but  $\bar{\chi}$  is positive and usually larger, about  $10^{-4}$ . Paramagnetism is common in dilute transition-metal salts, in which the metal ions with unpaired electrons interact with one another only weakly. The spins are randomly oriented at finite temperatures but align slightly when a field is applied. Alignment becomes more difficult at high temperatures causing a decrease in susceptibility with temperature following the Curie law. *Superparamagnets* contain clusters of paramagnetic ions. Exchange interactions are strong within a cluster, but weak between clusters. Yet another type of paramagnetism is found in metals where the conduction electrons create temperature independent *Pauli paramagnetism*. The effect is caused by small changes in the band structure for electrons of opposite spin.

When spins interact appreciably, three types of ordered configurations occur: antiferromagnetism, ferromagnetism and ferrimagnetism. All three show Curie-Weiss Law behavior at high temperatures in the paramagnetic region. On cooling, the materials undergo a phase transition to a state in which the atomic dipoles are aligned, even in the absence of an applied field.

*Antiferromagnetism* is the most common of the three phenomena. In a simple collinear antiferromagnet, adjacent spins are aligned in antiparallel directions, producing zero net moment at zero field. Canted, spiral, and other more complicated antiferromagnetic arrays have also been observed. The magnetic susceptibility is small and field-independent, with a pronounced maximum near the transition temperature, called the Néel point. A few antiferromagnets such as FeCl<sub>2</sub> undergo spin reversal under applied fields, converting to ferromagnets with all spins aligned. Dysprosium and other materials with antiferromagnetic-ferromagnetic transitions exhibit peculiar field dependence, causing them to be classified as *metamagnets*.

The most useful magnetic materials are ferromagnets and ferrimagnets. Both possess a spontaneous magnetization which shows hysteresis under applied fields and disappears at the Curie temperature. The ordered spin array of a *ferromagnet* consists of parallel spins. Ferromagnets are rare among oxides, with only CrO<sub>2</sub>, EuO, and a few other examples. In a simple *ferrimagnet*, neighboring spins are antiparallel but are either unequal in size or unequal in number. A number of important ferrimagnetic materials are found in the spinel and garnet families.

*Parasitic ferromagnetism* is an effect found in  $\alpha\text{Fe}_2\text{O}_3$  and certain other antiferromagnets. A weak ferromagnetism caused by canting of the spins is permitted for certain magnetic space groups. Parasitic ferromagnetism disappears at the Néel temperature.

### 1. Diamagnetism

The magnetic susceptibility ( $\chi = M/H$ ) of a diamagnetic material is negative so that a diamagnet tends to move *out* of a magnetic field. Paramagnets possess positive susceptibilities and move *in*. Most compounds are weakly diamagnetic because of Lenz's law. A change in magnetic flux passing through an electric circuit induces a current which opposes the flux change by creating a field in the opposite direction. In atoms and molecules, the "electric currents" are created by electrons moving about the nucleus; an applied field causes changes in the orbits, inducing diamagnetism which disappears when the field is removed.



### 3. Crystal Field Theory

In oxides, transition-metal ions are most frequently found in octahedral or tetrahedral coordination. The surrounding anions, especially the nearest neighbors, profoundly effect the electronic configuration and hence the properties of the material. One of the most successful descriptions of this effect is "crystal field theory", a term used to describe the electrostatic environment around a cation in a crystal, or in solution. As ordinarily applied, crystal field theory considers only the first sphere of coordination; nearest neighbor anions are approximated as point charges and the effects of Coulomb potential on the  $d$ -electrons of the cation are calculated. The measurements to which the theoretical treatment can be related include optical absorption spectra, paramagnetic spin resonance absorption, magnetic properties, and thermodynamic properties such as lattice energy and reaction rates [4].

Most of the work on crystal field theory treats the energy changes within partially filled  $d$  or  $f$  shells. There are five  $d$ -orbitals which are equal in energy in the free ion. This degeneracy in energy is lifted when the atom interacts with surrounding electrons, as shown in Fig. 59. In octahedral coordination  $d_{xy}$ ,  $d_{yz}$ , and  $d_{xz}$ , the three  $t_{2g}$  orbitals, point between the anions. Because of coulomb repulsion between negative electrons and negative anions, this lowers their energy relative to the  $d_{x^2-y^2}$  and  $d_{z^2}$  orbitals which are directed toward the neighboring anions. Thus,  $t_{2g}$  orbitals are lower in energy than the  $e_g$  orbitals, and are filled first. The order of filling for common transition-metal ions is given in Table 18. For tetrahedral coordination, the order is changed because the  $e$  orbitals lie lower in energy than do the  $t_2$  orbitals, again because of repulsion effects.

The foregoing description implicitly assumes that crystal field splitting is not as large as the coulomb effects in the free ion, so that Hund's rules are obeyed in the solid state. Most transition-metal oxides and fluorides are high-spin compounds in which the total spin quantum number is maximized (Hund's first rule). This is not true for some low-spin salts of  $\text{Co}^{3+}$  and isoelectronic  $\text{Fe}^{2+}$ .

Crystal fields effect electron energies and therefore contribute to the internal energy and to the stabilization of structures. As an example, consider the site preference in spinels where divalent and trivalent ions are distributed over octahedral and tetrahedral sites. In a *normal* spinel,  $\text{M}^{2+}(\text{R}^{3+})_2\text{O}_4$ , divalent ions occupy all the tetrahedral sites and the octahedral sites are filled with trivalent cations. Inverse spinels,  $\text{R}^{3+}(\text{M}^{2+}\text{R}^{3+})\text{O}_4$ , are partially disordered: the tetrahedral sites are occupied by trivalent cations and equal numbers of di- and trivalent ions

### 3. Crystal Field Theory

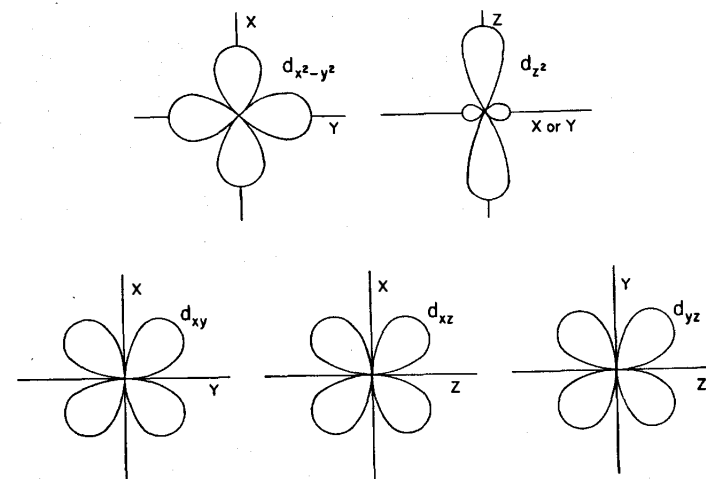


Fig. 59a. Geometry of the five  $d$ -orbitals

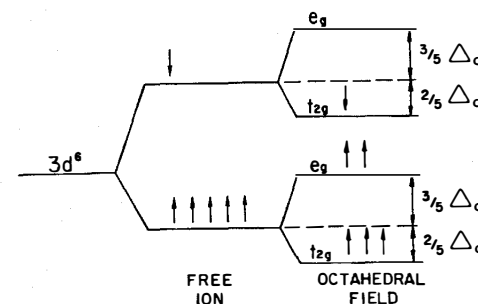


Fig. 59b. Ferrous iron  $\text{Fe}^{2+}$  energy levels in an octahedral field

are randomly distributed over the octahedral positions. The saturation magnetization is sensitive to the distribution as explained later.

Several factors are important in determining the type of ordering. Size considerations usually favor the inverse configuration because divalent ions tend to be larger than trivalent ions, and therefore prefer the larger octahedral site. On the other hand, coulomb energy slightly favors the normal form in which the electrostatic valence rule is exactly satisfied for every oxygen. Covalent bonding appears to be important for  $\text{Zn}^{2+}$  and  $\text{Cd}^{2+}$  which form  $sp^3$  hybrids and therefore prefer tetrahedral co-

ordination. Thus crystal field energy is only one of several energies involved, and it is perhaps surprising that it correctly predicts the configuration found in most transition-metal spinels.

There are two important groups of transition-metal spinels: the ferrites  $M^{2+}Fe_2^{3+}O_4$  and chromites  $M^{2+}Cr_2^{3+}O_4$ , where  $M^{2+} = Mn, Ni, Co, Fe$ , and  $Cu$ . All five chromites are normal spinels and all five ferrites inverse.

Crystal field stabilization energies for octahedrally and tetrahedrally-coordinated transition-metal ions are listed in Table 18. The way in which they are computed is illustrated in Fig. 59b using the  $Fe^{2+}$  ion in an octahedral field as an example. The crystal field lifts the free-ion degeneracy because the  $t_{2g}$  orbitals experience less overlap with the neighboring ions than do the  $e_g$  orbitals. Letting the energy separation between the  $t_{2g}$  and  $e_g$  states be  $\Delta_0$  (the octahedral crystal field parameter), the zero energy can be chosen as the weighted mean of the five  $d$  orbitals, so that the triple degenerate  $t_{2g}$  orbitals decrease by  $2\Delta_0/5$  and the  $e_g$  orbitals increase by  $3\Delta_0/5$ . The choice of zero is one of convenience, since the properties of interest depend on the splitting of the  $d$  orbital energies rather than their absolute magnitude, and is not meant to imply that the average  $d$ -orbital energy does not change when an ion is placed in an octahedral field. Returning to the  $Fe^{2+}$  ion, the stabilization energy for six  $d$  electrons in an octahedral field is  $4(-2\Delta_0/5)$  for the four  $t_{2g}$  electrons and  $2(+3\Delta_0/5)$  for the two  $e_g$  electrons, yielding a net decrease in energy of  $(-8/5 + 6/5)\Delta_0 = -2\Delta_0/5$ , as in Table 18. Generalizing this result for an atom with electron configuration  $(t_{2g})^n(e_g)^m$ , the stabilization energy is  $(-2\Delta_0/5n + 3\Delta_0/5m)\Delta_0$  for an octahedral field, and  $(+2n/5 - 3m/5)\Delta_T$  for tetrahedral coordination.

In the spinel problem, the site preference is determined by comparing the tetrahedral and octahedral stabilization energies. This requires relative values for the crystal field parameters  $\Delta_0$  and  $\Delta_T$ . As shown in Fig. 59, the  $d_{xy}$  orbital points exactly between neighboring anions while the  $d_{x^2-y^2}$  lobes are directed exactly toward them. Thus  $\Delta_0$ , the energy difference arising from  $d$  electron-anion repulsion in an octahedral field, is large. For tetrahedral coordination, the lobes are not directed exactly between or toward the neighboring anions, therefore the crystal field splitting is less, so that  $\Delta_T$  is less than  $\Delta_0$ . Calculations based on point charge models [4] have yielded the result  $\Delta_T = 4/9\Delta_0$ . Substituting this value for  $\Delta_T$ , octahedral stabilization exceeds that of the tetrahedral site for every ion except  $Fe^{3+}$  and  $Mn^{2+}$ , for which there is no stabilization energy in either case. The net stabilization energy is  $-0.84\Delta_0$  for  $Cr^{3+}$  and  $Ni^{2+}$ ,  $-0.42\Delta_0$  for  $Cu^{2+}$ ,  $-0.27\Delta_0$  for  $Co^{2+}$ , and  $-0.13\Delta_0$  for  $Fe^{2+}$ . Thus  $Cr^{3+}$  has a strong preference for octahedral sites while  $Fe^{3+}$  has none. Most of the divalent cations have a slight preference for

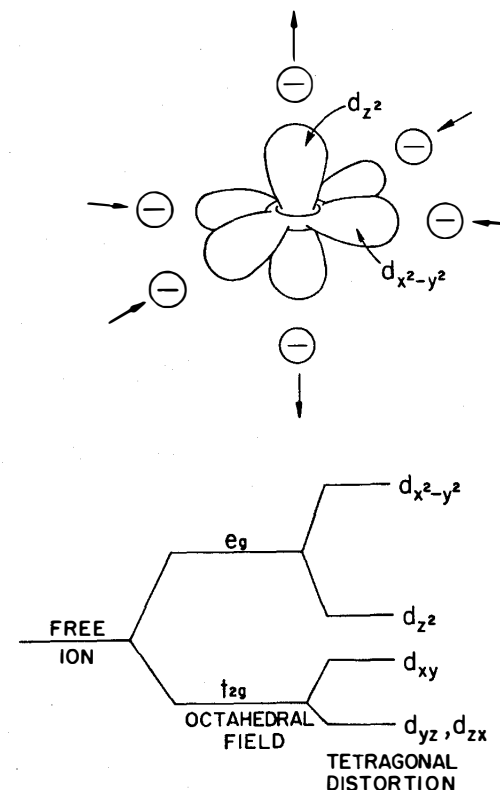


Fig. 60. The two  $e_g$  orbitals in a tetragonally-distorted octahedral field, and the resulting energy level diagram

octahedral coordination, explaining why the chromites are normal spinels and the ferrites inverse.

Additional stabilization energy can be obtained by deforming the environment of a transition-metal ion: the Jahn-Teller effect. Consider the two  $e_g$  orbitals in an octahedral field (Fig. 60). If the neighboring oxygen ions are shifted in the direction of the arrows, the two-fold degeneracy of the  $e_g$  orbitals is lifted. Under such a tetragonal distortion, the  $d_{z^2}$  orbital experiences less repulsion from the anion neighbors, lowering its energy relative to  $d_{x^2-y^2}$ . The distortion also lifts the

degeneracy on the  $t_{2g}$  orbitals, with  $d_{xy}$  raised slightly in energy because of the compression along  $x$  and  $y$ . The energy level scheme is illustrated in Fig. 60.

Whether or not such distortions lower the overall energy of the ion depends on the occupation of the orbitals, that is on the number of electrons. An ion with an orbitally-degenerate ground state can lower its energy by means of such a Jahn-Teller distortion. Thus the effect is often observed for  $d^4$  and  $d^9$  ions which contain an odd number of  $e_g$  electrons. Jahn-Teller distortions may also lead to sizeable long-range deformations since random deformations result in localized strain. Examples from the ferrite family include  $\text{Zn}[\text{Mn}_2]\text{O}_4$  and  $\text{Fe}[\text{CuFe}]\text{O}_4$  where the normally cubic spinel structures have tetragonal distortions of  $c/a = 1.14$  and  $1.06$ , respectively. The active Jahn-Teller ions in these compounds are  $\text{Mn}^{3+}(t_{2g}^3 e_g^1)$  and  $\text{Cu}^{2+}(t_{2g}^6 e_g^3)$ .

#### 4. Paramagnetic Salts

In transition-metal compounds, the distance between transition-metal ions determines whether or not long-range magnetic order occurs. In alums such as  $\text{KCr}(\text{SO}_4)_2 \cdot 12\text{H}_2\text{O}$ , the magnetic chromium ions are widely-spaced because of the intervening sulfate groups and water molecules, and the interactions between spins are small. The compounds remain paramagnetic to very low temperatures where the magnetic susceptibility becomes large in accordance with the Curie law. Alums and other dilute paramagnetic salts are used in cryogenic systems to achieve temperatures below  $0.001^\circ\text{K}$  by the process of adiabatic demagnetization.

The minimum temperatures achievable are limited by interactions either between paramagnetic electron spins, or between the electron and nuclear spins. Cerium is a good choice because the nuclear spin is zero, eliminating hyperfine interactions. Superhyperfine interactions are also small because the  $\text{Ce}^{3+} f$  electron shell is highly localized. For magnetically-dilute cerium salts, the minimum temperature is limited by dipole-dipole interactions between paramagnetic ions. Experiments [5] indicate that  $T_{\min}^2$  is proportional to the number of spins per unit volume. Cerium magnesium nitrate  $[\text{Ce}_2\text{Mg}_3(\text{NO}_3)_{12} \cdot 2\text{H}_2\text{O}]$ , cerium iodic antipyrine,  $[\text{Ce}(\text{C}_{11}\text{H}_{12}\text{ON}_2)_6\text{I}_3]$ , and cerium thiocyanate triphenyl phosphine oxide  $[\text{Ce}(\text{SCN})_3(\text{OP}(\text{C}_6\text{H}_5)_3)_4]$  are promising compounds for adiabatic demagnetization. Substituting non-paramagnetic ions for cerium leads to further dilution and further reduction in  $T_{\min}$ . Demagnetization experiments on  $(\text{Ce}_{0.1}\text{La}_{0.9})_2\text{Mg}_3(\text{NO}_3)_{12} \cdot 24\text{H}_2\text{O}$  gave temperatures of  $0.00086^\circ\text{K}$ .

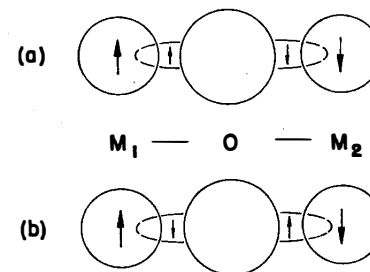


Fig. 61 a and b. The  $180^\circ$  superexchange interaction when the transition metal  $3d$  shell is (a) less than half full, and (b) half or more than half full

#### 5. Transition Temperatures

Magnetic-ordering occurs when the transition-metal atoms are nearest neighbors (metals) or next-nearest neighbors (simple compounds). Among oxides and fluorides, antiferromagnetism is much more common than ferromagnetism or ferrimagnetism. The reason is the superexchange interaction. Direct exchange seldom occurs in such materials because the transition-metal ions are not in direct contact, but interact *via* an intermediate anion. Superexchange is a strong interaction, leading to magnetic transition temperatures comparable to metals. Ferromagnetic ordering in Fe occurs at  $1040^\circ\text{K}$ , antiferromagnetism in  $\alpha\text{Fe}_2\text{O}_3$  at  $950^\circ$ , and ferrimagnetism in magnetite at  $860^\circ$ .

In the superexchange interaction two metal atoms  $M_1$  and  $M_2$  on opposite sides of an oxygen ion interact through a  $p$ -orbital of oxygen (Fig. 61). Transition-metal ions with less than half-full  $d$ -shells will be considered first. Since the oxygen ion is not fully ionized, its outer electrons spend time on the neighboring transition-metal ions. When it enters the  $d$ -shell of a transition-ion whose  $d$ -orbitals are less than half full, the oxygen electron spin is parallel to those of the metal ion, in accordance with Hund's rule. Meanwhile the other electron in the same oxygen  $p$ -orbital is on the opposite side of the oxygen ion because of the coulomb repulsion between two electrons in the same  $p$ -orbital. While there, the second electron (whose spin is antiparallel to the first electron because of the Pauli exclusion principle) also interacts with transition metal ions—and its spin will again be parallel to that of the metal ion if its  $d$ -shell is less than half full. The antiferromagnetic superexchange thus arises from the alignments as shown in Fig. 61: the first metal atom accepts an electron with parallel spin from an oxygen neighbor; the spins of the two electrons in the same oxygen  $p$ -orbital are antiparallel; and

the second electron spends part of its time in parallel alignment with the  $d$ -electrons of the second metal ion.

A similar situation is obtained when the  $d$ -electron shell of the transition metal ion is more than half full, again resulting in antiferromagnetic superexchange (Fig. 61). The oxygen electrons enter the metal atom  $d$ -shell antiparallel to the net spin, but since the same thing happens to the other electron, the interaction remains antiferromagnetic. Superexchange is strongest when the angle  $M_1-O-M_2$  is  $180^\circ$ , allowing maximum overlap of the  $p$ -orbital with the two metal ions. The interaction weakens as the angle approaches  $90^\circ$ , even though the metal-metal distance may be shorter.

Long range magnetic order disappears at high temperatures because of thermal disorder. The transition temperature is called the Curie point ( $T_c$ ) in a ferromagnet or ferrimagnet, and the Néel point ( $T_N$ ) in an antiferromagnet.  $T_c$  and  $T_N$  depend strongly on transition-metal concentration, as expected. The general trend is indicated by the transition temperatures for the following  $Fe^{3+}$  compounds, which are arranged in order of decreasing iron content:  $\alpha$ - $Fe_2O_3$  (958 °K),  $\gamma$ - $Fe_2O_3$  (743),  $FeOF$  (315),  $Fe_2MgO_4$  (653),  $Y_3Fe_5O_{12}$  (563),  $FeF_3$  (394),  $FeCl_3$  (10),  $Fe_2TeO_6$  (219),  $YFeO_3$  (643),  $FePO_4$  (25),  $Fe_3(PO_4)_2 \cdot 4H_2O$  (15),  $FeNH_4(SO_4)_2 \cdot 12H_2O$  (<1 °K). Magnetic interactions weaken with increasing dilution, although some noticeable irregularities occur in the list. The transition temperature of  $FeCl_3$  is surprisingly low, while that of  $YFeO_3$  is rather high. These exceptions illustrate the influence of crystal structure on the exchange interactions. Ferric chloride has a layer structure with sequence  $-Cl-Fe-Cl-Cl-Fe-Cl-$ . Neither direct nor superexchange interactions are possible between layers, hence  $T_N$  is very low. In  $YFeO_3$ , the arrangement of iron and oxygen are nearly ideal for  $180^\circ$  superexchange. The compound crystallizes in the perovskite structure with interconnected  $-O-Fe-O-Fe-O-$  chains in all three directions.

Magnetic transition temperatures for several series are plotted against ionization potential in Fig. 62. The ordering observed in these oxides and fluorides is due to superexchange interactions between transition-metal cations and intervening anions. The spin ordering temperature increases with ionization potential because the harder it is to ionize the cation (large IP), the more electron sharing there is between cation and anion. The only large deviations from this tendency are in ions with large spin-orbit interaction ( $Co^{2+}$  in octahedral fields and  $Ni^{2+}$  in tetrahedral fields). L-S coupling opposes spin alignment and therefore lowers the ordering temperature.

The ordering temperatures of compounds containing transition metal ions with shells less than half full are usually lower than comparable

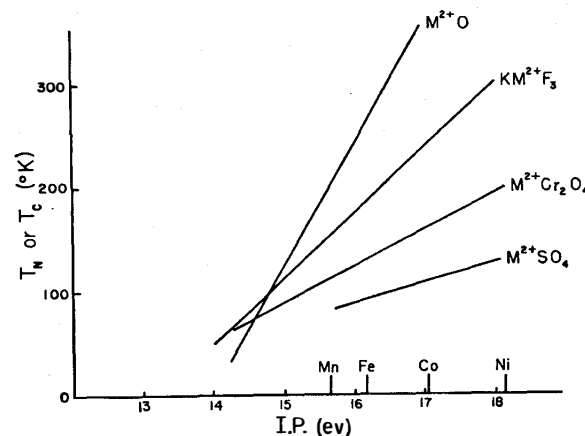


Fig. 62. Dependence of magnetic transition temperature on ionization potential of divalent transition metal compounds

compounds with ions whose shells are half-filled or more. Thus chromites have lower transitions than ferrites. The reason for this again has to do with the superexchange interaction and the fact that spin correlation between the paramagnetic ions rests upon the exclusion principle. If the electron shell of a high spin ion is already half full, then the spin direction of other electrons entering the shell must be opposite in direction.

Some interesting examples of one- and two-dimensional magnetic order occur in structures where the transition metal ions are arranged in chains or layers.  $CsNiF_3$  crystallizes in the hexagonal  $BaNiO_3$  structure.  $Ni^{2+}$  ions are octahedrally coordinated to six fluorines. The octahedra share faces and are arranged in chains along the  $c$ -axis. The  $Ni-Ni$  distances in the chain are 2.6 Å, whereas  $Ni$  ions belonging to neighboring chains are 6.2 Å apart. As temperature is lowered, ferromagnetic coupling within the chains sets in long before full three dimensional order. Only about 10% of the magnetic entropy is gained below  $T_c$  [6].

$MnTiO_3$  exhibits two-dimensional magnetic order above its Néel point. The structure is isomorphous with ilmenite with  $Mn^{2+}$  ions arranged in widely-spaced layers.

## 6. Magnetization

Magnetic moment is related to spin angular momentum, and in attempting to maximize  $M$  it is helpful to maximize  $S$ . Many useful magnetics are based on trivalent iron,  $Fe^{3+}$ , with its five unpaired

electrons. To take advantage of the large spins, they must be aligned to give a large macroscopic magnetization. But parallel spin alignment (ferromagnetism) is not easy to achieve in oxides because superexchange, the strongest interaction between spins, usually gives rise to antiparallel rather than parallel alignment. There are several ways to avoid antiferromagnetism.

One way is to look for a material with ferromagnetic exchange coupling. There are a few of these, notably  $\text{CrO}_2$ , a member of the rutile family which exhibits ferromagnetism below  $121^\circ\text{C}$ . The  $\text{Cr}^{4+}\text{--O--Cr}^{4+}$  interaction appears to be ferromagnetic in this compound because the intermediate anion overlaps full orbitals on one neighbor and empty ones on the other. Another example is the intermediate compositions in the perovskite series  $\text{LaMnO}_3\text{--CaMnO}_3$  in which the  $\text{Mn}^{3+}\text{--O--Mn}^{4+}$  interactions also give rise to ferromagnetism. The unusual ferromagnetic interaction in  $\text{La}_{1-x}\text{Ca}_x\text{MnO}_3$  has been traced to an electron-hopping mechanism. Manganese exists in two valence states in this material, giving rise to electron exchange between manganese ions. Electron spin remains unchanged during the transfer, making the interaction ferromagnetic. Competing antiferromagnetic interactions *via* localized electrons may lead to canting. Ferromagnetic oxides such as  $\text{CrO}_2$  and  $(\text{La}, \text{Ca})\text{MnO}_3$  are rare and usually involve unstable valence states.

Ferrimagnets are more common than ferromagnets and also possess large magnetization. In ferrimagnetic materials, the exchange coupling is antiferromagnetic but the two sublattices are unbalanced in magnetic moment so that a net magnetization results. If we confine attention to the simple collinear magnetic structures in which spins are directed either parallel or antiparallel to the direction of easy magnetization, then there are two ways of creating an unbalanced moment. One way depends on using two different transition metal ions.  $\text{NiMnO}_3$  is a ferrimagnetic material with the ilmenite structure, a corundum derivative. There are strong antiferromagnetic  $\text{Ni}^{2+}\text{--O--Mn}^{4+}$  interactions in  $\text{NiMnO}_3$  resulting in the Ni spins pointing antiparallel to the manganese spins, and since the moments of the ions are unequal, ferrimagnetism results.

Another more useful way of making ferrimagnets is to couple two sublattices which are unequal in number. Ferrites with the spinel structure are good examples. In spinel there are twice as many cations in octahedral environment as in tetrahedral. When transition metal ions occupy both sites, as in magnetite, there is a strong antiferromagnetic superexchange coupling between the tetrahedral and octahedral ions (Fig. 63). This is the dominant exchange interaction because it makes best use of the oxygen *p*-orbitals, but there are other interactions as well. The octahedral ions interact weakly with one another, an antiferro-

magnetic interaction that becomes important when the tetrahedral-octahedral interaction disappears. In the spinel ferrites, the spontaneous magnetization is equal to the *difference* between the sublattice magnetizations associated with octahedral and tetrahedral ions. By judicious choice of ions, the difference can be made quite large, and leads to an unusual situation in which adding a *nonmagnetic ion increases the magnetization*. This type of substitution has been used in the development of ferrite memory cores. Zinc ferrite ( $\text{ZnFe}_2\text{O}_4$ ) is a normal spinel whereas most of the other spinel ferrites have the inverse structure. Thus in a solid solution of  $\text{Ni}_{1-x}\text{Zn}_x\text{Fe}_2\text{O}_4$ , as *x* is increased,  $\text{Zn}^{2+}$  replaces  $\text{Fe}^{3+}$

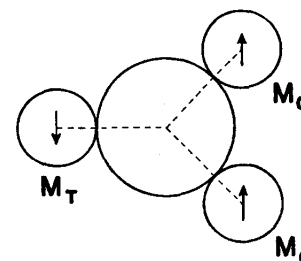


Fig. 63. Antiferromagnetic super-exchange between tetrahedral ( $M_T$ ) and octahedral ( $M_O$ ) transition-metal ions in the spinel structure

in the tetrahedral sites and  $\text{Fe}^{3+}$  fills the octahedral sites emptied by  $\text{Ni}^{2+}$ . Divalent zinc has no unpaired electrons, divalent nickel has two and trivalent iron five. Therefore as *x* increases, the magnetization of the tetrahedral sublattice is decreased while that of the octahedral sublattice increases, resulting in a large difference and a larger net magnetization [7]. The magnetization continues to rise with increasing zinc content until there are so few  $\text{Fe}^{3+}$  ions remaining in tetrahedral sites that the coupling between tetrahedral and octahedral ions breaks down and the weaker coupling between octahedral sites takes over giving rise to antiferromagnetism in pure  $\text{ZnFe}_2\text{O}_4$ .

## 7. Crystalline Anisotropy

Experimentally it is found that spontaneous magnetization tends to lie along certain crystallographic axes, an effect known as crystalline anisotropy. The atomic moments in ferromagnetic iron are aligned along

the [001] direction. Body-centered cubic  $\alpha$ -Fe has near-neighbor bonds directed along  $\langle 111 \rangle$  directions. In a cubic environment such as this the unpaired 3d electrons show a preference for the  $e_g$  orbitals pointing along  $\langle 100 \rangle$  directions. Magnetic moments align along these directions because of coupling between electron spin and unquenched orbital moment. Nickel is also ferromagnetic, and here the moments are parallel to a [111] direction. Ni is face-centered cubic with Ni-Ni bonds along  $\langle 110 \rangle$  directions. The  $t_{2g}$  orbitals directed along  $\langle 111 \rangle$  directions are favored under these conditions.

Anisotropy is defined as the work required to reorient the magnetization from the easy direction to another direction. It is customary to express anisotropy energy as a power series in the direction cosines ( $\alpha_1, \alpha_2, \alpha_3$ ) between the measurement direction and the crystallographic axes. For pseudocubic magnetic crystals, the leading term in the power series is  $K_1(\alpha_1^2\alpha_2^2 + \alpha_1^2\alpha_3^2 + \alpha_2^2\alpha_3^2)$ . For Ni, the  $\langle 111 \rangle$  body diagonals are the easy directions and  $K_1$  is negative.  $K_1$  is positive in Fe which magnetizes along  $\langle 100 \rangle$  directions. For most ferrites  $K_1$  is small and negative — but in  $\text{CoFe}_2\text{O}_4$  it is large and positive. Cobalt can be used as an additive to increase anisotropy and coercive field.

The strong preference of  $\text{Co}^{2+}$  spins for certain crystal axes appears to be related to its orbital degeneracy. The two ions with the greatest orbital degeneracy in octahedral sites are  $\text{Fe}^{2+}$  and  $\text{Co}^{2+}$ . Since the orbital configuration can be changed without changing the energy, the degenerate state possesses appreciable angular momentum.

In the spinel structure the octahedral sites are only approximately octahedral in symmetry. The true point symmetry of the so-called octahedral site is not  $m\bar{3}m$  but trigonal, crystal class  $\bar{3}m$ . Nearest and next-nearest neighbors are illustrated in Fig. 64. The next-nearest metal atoms superposed a trigonal field (with principal axis along  $\langle 111 \rangle$ ) on the octahedral field created by the oxygens. As a result the triple degenerate  $t_{2g}$  orbitals are split into a doublet and a singlet. The doublet wave functions lie principally in the plane perpendicular to [111], while the singlet extends parallel to [111]. Since the second nearest neighbors, six octahedral cations, are grouped close to [111], the singlet orbital is lower in energy because of the attraction between electrons and cations. Therefore, the energy level diagram is that shown schematically in Fig. 64.

In the case of  $\text{Fe}^{2+}$ , five electrons go in with spin up, one with spin down. The latter is in the single degenerate ground state so that  $\text{Fe}^{2+}$  has no orbital angular momentum in the ground state. For  $\text{Co}^{2+}$ , which has one more electron, the extra electron occupies half the doubly degenerate state. Therefore  $\text{Co}^{2+}$  is free to change its state in the plane perpendicular to [111], giving the atom angular momentum parallel to [111]. The

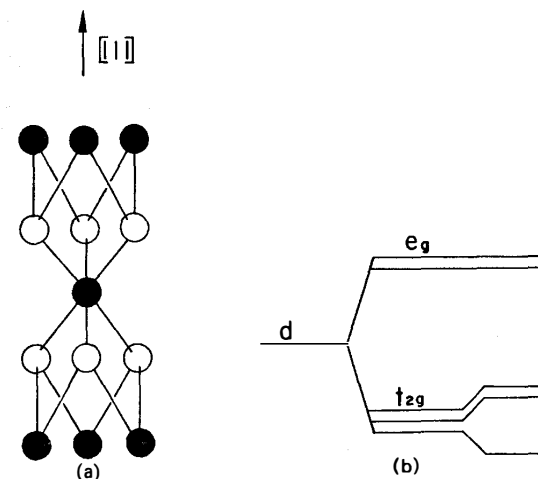


Fig. 64. (a) Environment of the octahedrally coordinated cation in the spinel structure, metal ions and oxygen are denoted by solid and open circles, respectively. (b)  $d$  orbitals for an octahedrally coordinated transition metal ion in a slightly trigonal field

angular momentum is fixed in direction and, because of spin-orbit coupling, the spin magnetic moments are also strongly aligned along [111]. This explains why the anisotropy constant of  $\text{CoFe}_2\text{O}_4$  is of opposite sign and larger than those of the other ferrites. SLONCZEWSKI used this explanation to explain magnetic anisotropy and magnetic annealing in ferrites [8]. In Fe-Co ferrite ceramics annealed in a magnetic field,  $\text{Co}^{2+}$  ions diffuse to sites in which the trigonal axis is closest to the applied field direction. Upon cooling the unbalanced  $\text{Co}^{2+}$  distribution is retained giving rise to uniaxial anisotropy.

There are other ways to create magnetic anisotropy in addition to cobalt additions. One way is through poling, another is compositional gradients, and a third is through shape anisotropy. The iron oxide used in magnetic tape,  $\gamma\text{-Fe}_2\text{O}_3$ , provides an example of the imaginative use of crystal chemistry in providing shape anisotropy through topotaxy.

Single-domain acicular particles of  $\gamma\text{-Fe}_2\text{O}_3$  oriented parallel to the length of the tape are the magnetic constituent of most recorders. When prepared with particle lengths about  $0.5\mu$  and length-to-width ratios about five,  $\gamma\text{-Fe}_2\text{O}_3$  particles behave like single domain arrays. But it is not easy to prepare cubic materials such as  $\gamma\text{-Fe}_2\text{O}_3$  in fine-grained



acicular (needlelike) morphology to develop the required shape anisotropy. The solution is pseudomorphism, the retention of crystal habit during conversion of one compound to another. Pseudomorphism is fairly common in mineralogy (limonite after pyrite is an example) and can be used to good advantage in synthetics as well.

Beginning from a ferrous salt solution, precipitation conditions are carefully controlled to give  $\alpha$ -FeOOH, an orthorhombic crystal of acicular habit. The ferric oxyhydroxide is gently oxidized to  $\alpha$ -Fe<sub>2</sub>O<sub>3</sub>, then reduced to magnetite Fe<sub>3</sub>O<sub>4</sub>, and finally oxidized again to  $\gamma$ -Fe<sub>2</sub>O<sub>3</sub>, retaining the original habit. Firing temperatures do not exceed 250° to 400° C. Magnetic  $\gamma$ -Fe<sub>2</sub>O<sub>3</sub> is slightly superior to magnetite because the latter exhibits oxidation and magnetic accommodation—making it difficult to erase a recording.

Improvements in the magnetic properties of polycrystalline materials have been achieved by controlling the directional alignment of the crystallites. In textured materials the crystallites have reasonably good alignment. There are several different ways of developing texture. Directional solidification is most suitable for brittle materials which cannot be mechanically deformed. By withdrawing heat in one direction from a molten metal, crystals grow from the cool side, following the direction of heat in the mold. Alnico and other permanent magnet materials are often cast by directional solidification.

Wire drawing, rolling and other deformation processes are used to produce texture in ductile materials. During deformation, the slip planes slide past each other, causing the crystals to assume a common directional alignment. The degree of control over the texture depends on the number of slip planes and the deformation technique. By adjusting die sizes, or the spacing between rollers, the metal is reduced in stages, leading to different textures.

The Permalloy tape used in sensing binary information in the magnetic twistor memory is produced by working and drawing the cast ingot into a fine wire, and then flattening it by rolling. Annealing treatment is also required to obtain a square hysteresis loop. Texture is important in eliminating magnetostriction [9].

## 8. Hard and Soft Magnets

Ferromagnetic and ferrimagnetic substances are classified as hard and soft magnetic materials in regard to their hysteretic characteristics. Hard magnets are used as permanent magnets in loudspeakers and meters, while soft magnets are used as transformer cores and in motors

and generators. The hysteresis loop of a soft magnet is characterized by high magnetic permeability and low coercive field to reduce energy loss. Almost all the opposite properties are desired in a hard magnet. Coercive fields range from about 0.1 A/m in supermalloy to more than  $2 \times 10^5$  A/m in FePt. Permeabilities also cover about six orders of magnitude.

Iron-silicon alloys containing 1–5% Si are widely used for transformers and rotating machinery. Silicon improves the magnetic properties of iron by reducing the crystalline anisotropy and coercive field, but high silicon alloys are brittle and hard to work. Another way to reduce the anisotropy is to align the grains with easy directions parallel to the direction of magnetization. This is accomplished by a sequence of rolling and annealing operations.

Iron-nickel alloys are superior to silicon steels as soft magnets, but are rather expensive. Permalloy and supermalloy both contain about 80% Ni. Crystalline anisotropy and magnetostriction are very small for such compositions, and by adding a small amount of molybdenum, both effects disappear. Supermalloy is made up of 79% Ni, 16% Fe, 5% Mo.

Eddy current loss is of primary importance in high frequency applications. The high resistivity of Ni–Zn and Cu–Zn ferrites together with their high permeabilities make them more suitable than metals.

Alnico V is representative of the alloys used for permanent magnets. As the name suggests, Alnico contains Al, Ni, and Co, in addition to Fe and Cu. On slow cooling from 1300° C the alloy segregates into two finely-divided precipitates, which is the origin of the high coercivity.

Another widely-used hard magnetic material is barium ferrite. BaFe<sub>12</sub>O<sub>19</sub> is a ferrimagnetic oxide with the magnetoplumbite structure, a close-packed structure with a large hexagonal unit cell. The big Ba<sup>2+</sup> and O<sup>2-</sup> ions form the close-packed array with Fe<sup>3+</sup> distributed over octahedral, tetrahedral and trigonal bipyramid interstices. The schematic representation of the structure shown in Fig. 65 points out the similarity to spinel. Saturation magnetization is also similar to the spinel ferrites but the crystalline anisotropy is much larger because of the lower symmetry. Spins are locked tightly to the [001] direction giving a high coercive field. Magnetic hotpressing is effective in aligning the easy axes of fine-grained barium ferrite ceramics [7].

Rare earth-cobalt permanent magnet alloys are a relatively recent development [10]. Previously unattained coercivities have been achieved with R Co<sub>5</sub> (R = Y, Ce, Pr, Nd, Sm) intermetallic compounds. These and a number of other rare earth compounds with Co, Ni, and Cu have the CaCu<sub>5</sub> structure type (Fig. 66). For the cobalt compounds with yttrium and the light rare earth elements, the R sublattice is coupled ferromagnetically to the magnetization of the Co sublattice giving high saturation magnetizations and the largest known crystalline anisotropy.

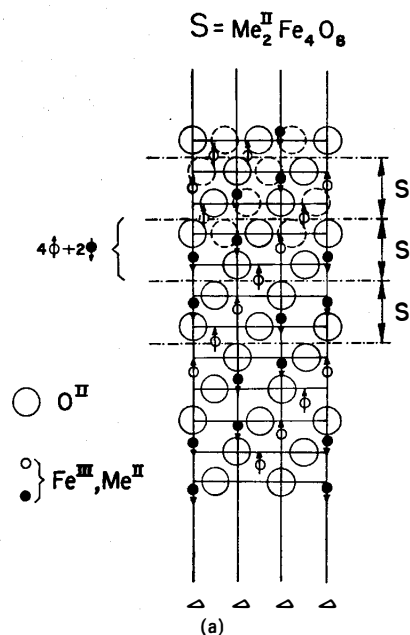


Fig. 65a. Cross-section through a mirror plane of the spinel structure with the  $[111]$  axis vertical, drawn for the ideal value of the parameter  $u$ . The vertical lines are axes of threefold symmetry. All ions not lying on one of these axes occur three times, as shown schematically by broken circles in the top layers. The small white and black circles represent respectively ions on octahedral and tetrahedral sites. The arrows indicate the relative orientation of the magnetic moments of the ions on these sites [7]

## 9. Bubble Memories

Among the more important magnetic devices are the cores, disks, and tapes used in digital computers to store information. The recently developed bubble-domain devices can do logic, counting, and switching, as well as memory storage, all at high speeds in a small space. For almost two decades, ferrite memory cores have dominated the computer field, although it now appears that several other systems offer competitive alternatives. Ferrite core arrays are well-suited to random access memory, and adaptive high-speed memory. Cycle times are about  $1\mu\text{sec}$ , with power dissipation levels near  $100\mu\text{W/bit}$  and adequate reliability.

Competing systems are based on integrated circuits, magnetic bubbles, and charge-coupled devices [11]. Semiconductor memories got

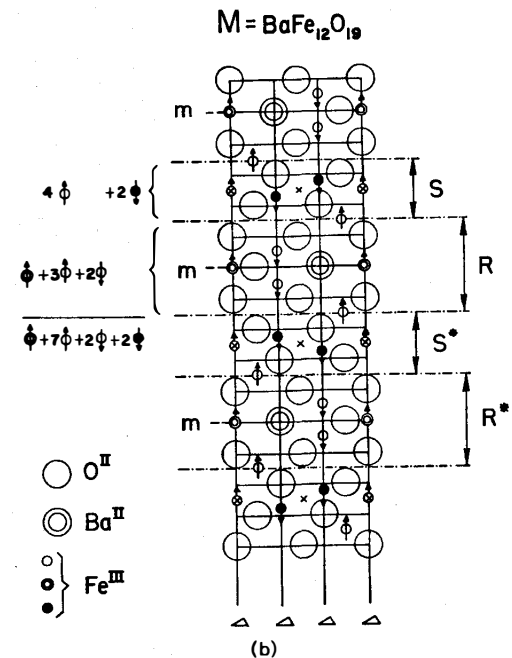


Fig. 65b. Cross-section of the magnetoplumbite structure  $M$ , with the  $c$  axis vertical. The arrows indicate the spin orientations. The drawn vertical lines are axes of threefold symmetry. A cross indicates a centre of symmetry. All layers containing barium are mirror planes, and are denoted by  $m$ . This structure consists of the same  $S$  blocks as in Fig. 65a. separated by  $R$  blocks containing barium. The asterisk indicates a rotation of a block by  $180^\circ$  about the  $c$ -axis [7]

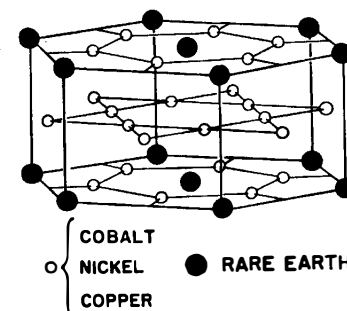


Fig. 66. Intermetallic compounds such as  $\text{SmCo}_5$  have the  $\text{CaCu}_5$  structure. Spins are locked along the hexagonal  $c$ -axis making them excellent permanent magnets

started with the flip-flop circuit. Integrated circuit memories now excel core memories in speed and are within striking distance in cost, power and reliability. Circuit innovations and new electron- and ion-beam processes are capable of producing chips containing  $10^4$  bits. The disadvantage is that fabrication methods require a large number of complex processes to produce the desired circuitry in silicon. A phenomenon requiring fewer steps might offer a more adaptive technology.

Magnetic bubbles constitute a system of identical particles which can do logic, memory and switching without altering the homogeneous host material. The bubbles are  $180^\circ$  cylindrical magnetic domains which can be created and destroyed, and moved reversibly in two dimensions.

Charge-coupled devices are related in concept to magnetic bubbles. Regions of charge are manipulated in a semiconductor just as domains are manipulated in a magnetic material. In both cases, the electrode geometries are simple and excellent bit-densities will be achieved when electron-ion processing is introduced. Bubbles will have the lower cost.

Magnetic bubbles are  $180^\circ$  cylindrical domains, about  $1\ \mu$  in diameter which can be created, moved about, divided, and destroyed by applied bias-fields. The experiments are carried out in thin magnetic plates with the spontaneous magnetization perpendicular to the plate. This is not possible under ordinary circumstances because of the large demagnet-

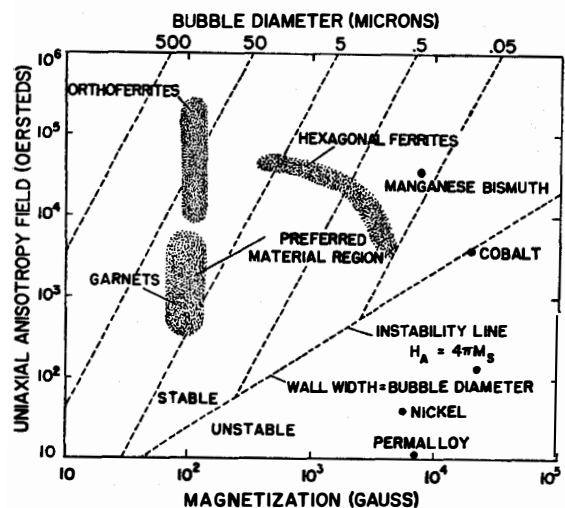


Fig. 67. Desirable bubble domain materials have bubble diameters near  $10\ \mu$ . Garnets cluster closest to the preferred region [12]

izing field created by surface magnetic charge; only in materials in which the anisotropy field exceeds the demagnetizing field are such domains stable. Mathematically, the stability criterion is  $H_A \geq 4\pi M_s$ , where the anisotropy field  $H_A$  is measured in oersteds, and  $M_s$  is the saturation magnetization in gauss. This is one of the few instances in which a *small* magnetization is desirable. Most magnetic materials, including iron and the ferrimagnetic spinels, do not satisfy this requirement (Fig. 67).

Bubble domains were first observed in hexagonal barium ferrite, a member of the magnetoplumbite family. These materials are often used as permanent magnets because of their large anisotropy, but the bias fields required for bubble domain devices are too large. Rare-earth orthoferrites with the perovskite structure and rare-earth garnets are much more practical because the magnetizations are smaller, and so are the required bias fields. In the orthoferrites a small magnetization is obtained by making use of parasitic ferromagnetism, a weak ferromagnetism accompanying antiferromagnetics with certain magnetic symmetry. In  $\text{GdFeO}_3$  the  $\text{Fe}^{3+}$  spins are antiferromagnetically coupled, with the spin axis nearly parallel to  $a$ . A small ferromagnetic component along  $c$  is allowed because it does not violate the symmetry conditions of the magnetic space group. Other parasitic ferromagnets might also prove useful in bubble domain devices.

The rare-earth garnets make use of different principles. Magnetization is made small by substituting Ga for Fe in the tetrahedral sites, and an anisotropy field is created by ordering of rare-earth ions during crystal growth or under mechanical stress. Gradients in the rare-earth ion concentration leads to anisotropic exchange interactions and sizeable anisotropy fields. The garnets have smaller bubbles than the orthoferrites, allowing higher information density. Magnetic rare-earth garnets support micron sized bubbles and can be grown epitaxially on gadolinium gallium garnet and other high-quality crystalline substrates.

Preferred properties of bubble materials are shown in Fig. 67. It is first of all essential that the material be uniaxial: magnetizable only along a single axis. The greater the uniaxial anisotropy field the more stable the unique magnetic axis. When this field is high, however, the bubbles tend to have too large a diameter. If the field is too low, there is a danger that zones of reverse magnetization will nucleate spontaneously. Garnets seem to cluster closest to the preferred region.

Amorphous metallic films show promise for bubble domain devices and certain magneto-optic applications. Gd-Co and Gd-Fe films prepared by sputtering from arc-melting targets show a surprising amount of perpendicular uniaxial anisotropy, despite the absence of crystallinity. The saturation magnetization at room temperature can be

varied over a wide range by changing the composition of the film. The variation in magnetization with composition has been attributed to anti-ferromagnetic exchange coupling between rare-earth and transition-metal atoms. Compensation occurs at a critical temperature where the magnetization of the rare earths cancels that of the transition metals, similar to the behavior of rare-earth garnets. Compensation temperatures between 40° and 500° K have been obtained in amorphous gadolinium-cobalt alloys.  $Gd_{0.2}Co_{0.8}$  films are useful in thermomagnetic writing and erasing since the compensation temperature is near room temperature. Compared to polycrystalline films, the principal advantage of the amorphous films is large signal-to-noise ratio. Grain noise is negligible in amorphous materials.

Amorphous bubble memories are inexpensive compared with crystalline films. Bubbles of 0.1  $\mu$  diameter have been observed, and if appropriate circuit masks can be developed, information densities of one billion bits per  $cm^2$  are possible. Unfortunately the domain memories are thus far limited to submillisecond access times; far slower than required memory speeds.

## 10. Microwave Garnets

The design of microwave ferrimagnetic garnets illustrates how magnetic properties can be optimized by chemical composition. Though cubic, the garnet structure (Fig. 68) is rather complex with three types of cation sites. Gadolinium iron garnet ( $Gd_3Fe_5O_{12}$ ) is a typical magnetic garnet. Three out of five  $Fe^{3+}$  ions are in tetrahedral positions, with the remainder in octahedral coordination. Gadolinium is in dodecahedral coordination with four oxygen neighbors at 2.38 Å and four more at 2.44 Å. Ferric iron is octahedrally coordinated to six oxygens at 2.00 Å, slightly larger than the tetrahedral Fe-O distance of 1.88 Å. Every oxygen is coordinated to two yttrium and two iron, one octahedral and one tetrahedral. Iron atoms in the octahedral and tetrahedral sites are coupled antiferromagnetically by the superexchange mechanism. Gadolinium is weakly coupled to the net moment of the iron atoms, again antiferromagnetically. Because of its large moment and weak coupling, gadolinium contributes little to the saturation magnetization at high temperatures, but tends to dominate at low temperatures. Between these two extremes the magnetization changes sign, the so-called compensation temperature.

Microwave devices such as resonance isolators, junction circulators, and phase shifters depend on ferromagnetic resonance, in which energy

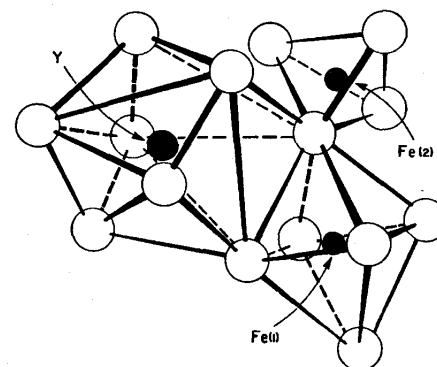
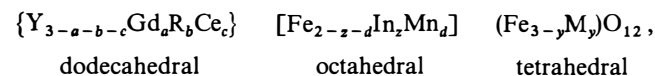


Fig. 68. Partial structure of Yttrium Iron Garnet (YIG) illustrating the coordination of the various cations with oxygen

from a circularly polarized radio-frequency wave sustains precession of unpaired electrons about an applied static magnetic field. In these devices it is important to control the magnetization and its variation with temperature, as well as the resonance and remanence properties, and the high-power characteristics. Optimization has been demonstrated [13] with garnets of composition



where  $R = Dy, Ho$  or  $Tb$ , and  $M = Al$  or  $Ga$ .

The saturation magnetization is increased by substituting  $In$  in the octahedral site and decreased with  $Ga$  or  $Al$  in the tetrahedral site. The operating range of the device is broadened by making  $dM/dT$  small; and is accomplished by  $Gd$  substitution in the dodecahedral site. Insertion loss, bandwidth, and phase shift are partially controlled by the combined influence of rare-earth,  $In$  and  $Al$  substitution on the resonance linewidth. The spin-wave linewidths determining the maximum power level are increased when  $Ho, Tb$  or  $Dy$  are substituted for  $Y$ . Magnetostrictive effects are strongly influenced by  $Ce$  and  $Mn$  substitutions. Each of these substitutions has side effects—sometimes undesirable side effects—so that a “tailor-made” composition for a high-power device differs from those with large bandwidth.

## 11. Magneto-optic Materials

The development of magneto-optic memory systems and of magneto-optic light modulators has revived interest in the Faraday effect and related phenomena. The polarization direction of light transmitted through a magnetic crystal undergoes a rotation proportional to the projection of the magnetization on the direction of propagation, an effect discovered by Faraday in 1845. Rotation can be observed in reflection as well as transmission, the Kerr effect. Magneto-optic rotation can be induced in dia- and paramagnetic materials with an applied field but the effects are small compared to ferromagnets since the rotation is proportional to magnetization.

Magneto-optic memories offer a promising method for information storage in computers. They combine the high-bit density of optical recording with the best features of magnetic storage, permanence and ease of erasability. Information is stored through the mechanism of Curie point writing in which light is absorbed in a magnetic film, thereby heating the film. Regions of the film under intense illumination revert to the paramagnetic state when heated above the Curie point. When cooled in a suitable magnetic field, the paramagnetic region returns to a magnetized state, but the direction of magnetization is changed. The resulting domain pattern mimics the incident light beam. Information is read either by reflected light (the Kerr effect) or by transmitted light (the Faraday effect).

Requirements for a useful storage medium are high bit-density, high write-sensitivity and high read-out efficiency [14]. Bit-density is determined by minimum domain size, so that a large magneto-crystalline anisotropy is needed for thin-film configurations. Important material parameters for Curie-point writing include low thermal conductivity, a convenient Curie point, and high optical absorption. Large heavy atoms favor low thermal conductivity as well as large Faraday rotation. Large magneto-optic effects are necessary for read-out efficiency. To avoid deleterious birefringence effects, it is advantageous to direct the light beam along an optic axis. This is easiest in uniaxial materials in which the magnetization is directed parallel to the symmetry axis. The spin-orbit interactions found in materials with heavy atoms of high atomic number give rise to large Faraday rotations. Of these materials, ferromagnetic MnBi and EuO appear to be the most interesting. The magneto-optic effects in magnetic metals and intermetallic compounds are about a hundred times larger than in most ferrites. This is the chief advantage of permalloy and cobalt over gadolinium iron garnet and yttrium iron garnet. Fine-grained ferromagnets consisting of

an array of submicroscopic ferromagnetic grains embedded in an insulating matrix appear particularly promising.

Like magnetization, large magneto-optic effects arise from the spins of unpaired electrons. Electron orbital motion is locked to the spins through spin-orbit coupling, giving precession about the magnetization direction. Light incident upon the crystal divides in right and left circularly polarized waves which travel with different rates of speed in a magnetic material depending on their orientation with respect to electron orbital motion. On leaving the crystal, the waves recombine to give a plane-polarized light, but the plane of polarization is rotated from its original position. The specific rotation, measured in degrees rotated per unit thickness, is large in ferro- and ferrimagnetic materials. Iron, cobalt, and nickel produce rotations of almost a million degrees/cm, but these materials are opaque in thicknesses greater than 1000 Å, so that transparent magnetic materials are needed. Ferromagnetic  $\text{CrCl}_3$  and  $\text{CrBr}_3$ , are transparent in the visible but must be operated at liquid He temperatures because of their low Curie points. The same objection applies to EuSe and other divalent Eu salts. This is unfortunate, since  $\text{Eu}^{2+}$  gives rise to large magneto-optic rotations because of its large spin-orbit effects and the proximity of the  $4f-5d$  electronic transition. Like the refractive index, specific magneto-optic rotation is greatly enhanced by certain optical transitions, so much so that it can be used as a spectroscopic tool.

Garnets appear to be the best magneto-optic materials at present. Depending on wavelength and composition, the specific rotation of ferrite garnets lies in the range 200–2000° C/cm in the near infrared. Gadolinium iron garnet operated near the compensation temperature (14° C) has been used in memory systems with optical access, performing both the read and write functions. High information density is possible in such systems since electric or mechanical access is unnecessary.

The magneto-optic modulator illustrated in Fig. 69 makes use of the fact that the Faraday effect is zero when the material is magnetized per-

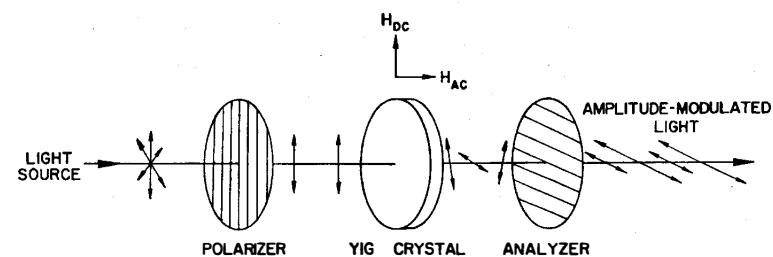


Fig. 69. Magneto-optical light modulator [15]

pendicular to the light beam. A thin slice of yttrium iron garnet is placed in a microwave cavity and magnetized perpendicular by an external D-C magnetic field. A microwave signal will then produce a component of magnetization parallel to the light beam, which in turn produces rotation of plane of polarization of the light beam, allowing light through the analyzer. The intensity of the light beam varies synchronously with the modulating microwave field. Modulation frequencies up to the gigacycle range are possible, but new magneto-optic materials with large Faraday effects and high transparency are needed.

## 12. Magnetoelectricity

One of the patterns in solid state research over the past decade has been the trend toward the interrelation of various physical phenomena. Magneto-optic, magnetoelectric, piezomagnetic, magnetostrictive, and various galvanomagnetic effects have been the subjects of numerous investigations, and the trend will probably continue. Several of these phenomena exhibit ferroic behavior and were discussed in an earlier section.

The magnetoelectric effect is especially interesting because it introduces a hitherto unsuspected connection between electric and magnetic forces. For  $\text{Cr}_2\text{O}_3$  and other magnetoelectric materials, an applied magnetic field not only induces magnetization, but electric polarization as well. The inverse phenomenon, electrically-induced magnetization occurs as well.

An atomistic origin of the magnetoelectric effect is illustrated in Fig. 70. Consider the electrically-induced magnetoelectric effect in an antiferromagnetic crystal. Initially with no applied field, both the net magnetization and the electric polarization are zero. When a field is applied parallel to the chain direction, positive ions move in the field direction and negative ions are displaced in the opposite direction, creating electric polarization. For the configuration in Fig. 70, cation and anion move closer together in one pair and further apart in the other. The resulting increase or decrease of atom overlap will affect the electron orbital motion in the cations, changing their magnetic moments.

Since "up" moments are differently affected than "down" moments, the net magnetization is no longer zero. Thus an applied electric field induces magnetization, the magnetoelectric effect.

Note that the model in Fig. 70 possesses a center of symmetry accompanied by time reversal,  $1'$ . All magnetic materials with a center of symmetry ( $1$ ) which is *not* accompanied by time reversal are non-

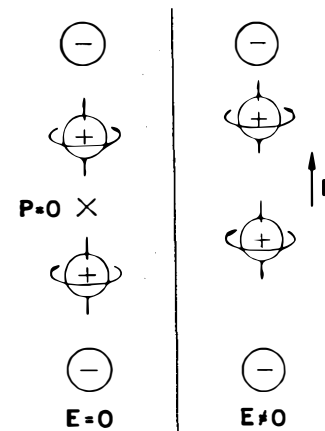


Fig. 70. One-dimensional model of the magnetoelectric effect in antiferromagnets. The cross shows the location of the  $1'$  center

magnetoelectric, eliminating ferromagnets like  $\alpha\text{-Fe}$ . This symmetry restriction is similar to that for piezoelectricity; all centric crystals are non-piezoelectric.

As described in Chapter IV, magnetoelectricity exists in materials with certain types of long-range magnetic order. The effect is absent in 32 of the 90 magnetic point groups. Measurements have been reported for about thirty magnetoelectric materials [16]. Coupling coefficients are small, limiting interest in device development, but the predicted behavior of light in magnetoelectrics warrants further investigation. Theoretical calculations predict nonreversible rotation of plane polarized light.

The possibility of magnetically-induced piezoelectricity and ferroelectricity has been suggested [17]. A reduction in symmetry accompanies the onset of long-range magnetic order. A material which is centrosymmetric in the paramagnetic state may lose the center when the spins align, thereby becoming a potential piezoelectric:  $\text{CaMn}_2\text{O}_4$  and a few other compounds possess the required symmetry change but the piezoelectric effect has yet to be demonstrated.

## References for Chapter VI

1. CHIKAZUMI, S.: Physics of Magnetism. New York: John Wiley and Sons 1964.
2. PAULING, L.: J. Chem. Phys. **4**, 673 (1936).
3. WERNICK, J. H.: Treatise on Solid State Chemistry, Vol. I, Chap. 4 (ed. N. B. Hannay). New York: Plenum Press 1973.

4. McCLURE, D.S.: Solid State Phys, Vol. 9, p. 399 (eds. F. Seitz and D. Turnbull). New York: Academic Press 1959.
5. ROACH, P.R., ABRAHAM, B.N., KETTERSON, J.B., GREINER, R., VAN ANTWERP, W.: J. Low Temp. Phys. **13**, 59 (1973).
6. LEBESQUE, J.V., SNEL, J., SMIT, J.J.: Sol. State Comm. **13**, 371 (1973).
7. SMIT, J., WUN, H.P.J.: Ferrites. New York: John Wiley and Sons 1959.
8. SLONCZEWSKI, J.C.: Phys. Rev. **110**, 1341 (1958).
9. CHIN, G.Y.: Bell Lab. Record **49**, 71 (1971).
10. WERNICK, J.H.: Ann. Rev. Mat. Sci., Vol.2, p.607 (ed. R.A. HUGGINS). Palo Alto, Calif.: Annual Reviews Inc. 1972.
11. MORTON, J.A.: Trans. I.E.E.E. MAG-7, 333 (1971).
12. BOBECK, A.H., SCOVIL, H.E.D.: Sci. Am. **224**, 78 (1971).
13. HUDSON, A.H.: Revs. Phys. in Tech. **1**, 9 (1970).
14. COHEN, R.W., MEZRICH, R.S.: R. C.A. Review **33**, 54 (1972).
15. ANDERSON, L.K.: J. Appl. Phys. **34**, 1230 (1963).
16. BERTAUT, E.F., MERCIER, M.: Mat. Res. Bull. **6**, 907 (1971).
17. GOSHEN, S., MUKAMEL, D., SHAKED, H.: J. Appl. Phys. **40**, 1590 (1969).

## VII. Materials with Useful Mechanical Properties

Inorganic solids are not very elastic. Cohesive strengths are typically 1% of the elastic modulus, which means that the solid elongates only a few percent before breaking. Elastic properties of oxides are nevertheless important in ceramic science and in the geosciences. Most minerals in the earth's crust are oxides and their stiffness moduli bear special relevance to our understanding of rock mechanics and seismic wave velocities. Recent developments in acousto-optics and surface waves have also generated interest in the elastic properties of oxides. New materials with unusual elastic behavior are needed for delay-lines and other electronic devices in which an electric signal is converted to an acoustic wave and subsequently re-converted to an electric signal. Elastic coefficients govern the velocity of the acoustic wave, and hence the transit time.

### 1. Elasticity

All solids change shape under forces. Under small stress, the strain  $\epsilon$  is related to the stress  $\sigma$  by Hooke's law ( $\sigma$ ) = (c)( $\epsilon$ ). The elastic stiffness coefficients (c) constitute a fourth rank tensor in which the number of independent coefficients depends on symmetry (Table 4). In concentrated matrix notation  $\sigma_i = c_{ij}\epsilon_j$ , where  $i, j = 1, 2, 3$  refer to longitudinal stresses and strains along axes  $X_1$ ,  $X_2$ , and  $X_3$ , respectively. For shearing motions about each of the axes,  $i, j = 4, 5, 6$ . The discussion which follows will be concerned mainly with the relative values of  $c_{11}$ ,  $c_{22}$ , and  $c_{33}$ , the coefficients relating change in length along a principal direction to a parallel component of stress. The shearing stiffness about the three principal axes are  $c_{44}$ ,  $c_{55}$ , and  $c_{66}$ .

Stiffness coefficients for many inorganic materials have been collected by HEARMON [1], SIMMONS [2], and HUNTINGDON [3]. From the results it appears that packing density is the primary variable affecting the elastic moduli of oxide compounds. BIRCH [4, 5] has shown that most common minerals have about the same mean atomic weight (molecular weight divided by the number of atoms in the chemical formula), and that longitudinal sound velocity is roughly proportional to density. Shear velocities also increase with rock density [6].